

Transducer for mechanical impedance testing over a wide frequency range through active feedback

Michael Wiertelowski^{1, a)} and Vincent Hayward^{2, b)}

¹⁾CEA LIST, *Sensory and Ambient Interfaces Laboratory, Fontenay-Aux-Roses, France.*

²⁾UPMC Univ Paris 06, UMR 7222, *Institut des Systèmes Intelligents et de Robotique, Paris, France*

(Dated: February 2012)

We describe a feedback-controlled active mechanical probe which can achieve a very low mechanical impedance, uniformly over a wide frequency range. The feedback produces a state of quasi-resonance which transforms the probe into a source of force used to excite an unknown load, resulting in a precise measurement of the real and imaginary components of the load impedance at any frequency. The instrument is applied to the determination of the mechanical impedance of a fingertip.

PACS numbers: 07.07.Mp, 45.80.+r, 62.40.+i

Keywords: Mechanical Impedance, Mechanical Resonance, Closed-loop Control, Transducer

I. INTRODUCTION

The present article describes an apparatus which is primarily intended for the measurement of the fingertip mechanical impedance, and of other objects of similar scale. The characterization of the bulk mechanical properties of the human finger plays an important role in the study of touch perception, in the design of tactile and haptic interface devices, in rehabilitation systems involving mechanical interaction of the hand with surfaces, and in other fields such as the detection of skin pathological conditions.^{1–8} For instance, the study of the stability and robustness of the control of haptic devices depends on such knowledge.⁹ Another example is in the area of tactile stimulators, where an accurate recording and reproduction of tactual signals depends on the knowledge of the mechanical characteristics of the skin.^{10,11}

The concept of impedance and of its inverse—the concept of mobility—is useful to model and analyze the dynamics of mechanical, electrical, acoustic, hydraulic systems, and combinations thereof.^{12,13} In the mechanical domain, one considers the relationship between the force applied to an element and the resulting displacement. When linear, lumped parameter analysis applies, an impedance can be represented by a combination of interconnected masses, springs, and dampers.

There are several approaches to measuring mechanical impedance. At the meso-scale, a widely used device is the so-called ‘impedance head’ employed in conjunction with an electrodynamic shaker. This device simultaneously records force and acceleration signals using two separate sensors. The inertial term resulting from the movements of the probing peg is subtracted from force readings in order to access force and acceleration at the interaction point. Measurements involve activating the shaker to excite the region or the object to be probed. Excitation

can also be achieved through inertial forces, rather than from ground reaction.¹⁴ Achieving collocated sensing, a prerequisite for accurate measurements, is difficult and collocation defects result in significant errors in the final impedance measurement.¹⁵ Another approach is to recover the mechanical impedance from the variation of the electrical impedance of an electromagnetic transducer which can be measured accurately.¹⁶

In nanotechnologies, the options are more limited. An approach to measuring mechanical properties at a very small scale is to use a vibrating cantilever driven at its natural resonance. The measurement then involves detecting amplitude changes for the same frequency (amplitude modulation) or the resonance frequency shift for the same amplitude (frequency modulation) of the tip of a cantilever in contact with a sample to be probed.^{17–20} This approach is particularly effective in vacuum since the Q-factor of the instrument, and hence its sensitivity, can reach large values. The displacement amplitude at resonance can then be much above the noise floor of the sensors, resulting in a high signal-to-noise ratio. Exciting a transducer at resonance is akin to reducing its impedance to a small value.

The instrument about to be described employs a resonance approach, yet, it is capable of operating over a wide range of frequencies, instead of just one. The system is driven by a closed-loop controller that reduces the apparent impedance of an electromagnetic transducer by almost an order of magnitude. Error propagation analysis shows how the feedback loop reduces measurement uncertainty. The impedance of the probed object can be recovered by subtraction of the unloaded response from the measurement made during testing.

The instrument is applied to produce frequency sweeps of the probing force to recover the impedance of a fingertip over a wide bandwidth. A complete measurement example is provided, revealing interesting properties of the mechanical behavior of the human fingertip.

^{a)}Electronic mail: michael.wiertelowski@cea.fr

^{b)}Electronic mail: vincent.hayward@isir.upmc.fr

II. IMPEDANCE MASKING APPROACH

In the foregoing, a symbol in capital case designates the Fourier transform of a signal identified by the corresponding lower case symbol. Capital letters also denote the Laplace transform of a transfer function.

A. Principle

Referring to Fig. 1, the apparatus comprises a force generator, $f(t)$, acting on the probe associated to an impedance, z_p , having a tuned response. The response is affected by coupling the probe to an unknown load impedance, z_u , e.g. a finger. If the two impedances share the same velocity by mechanical connection, recovering the unknown impedance involves subtracting z_p from the total impedance z . In frequency domain we have,

$$Z_u(j\omega) = Z(j\omega) - Z_p(j\omega), \quad \forall \omega \in B,$$

where ω is the pulsation and B is the frequency range considered.

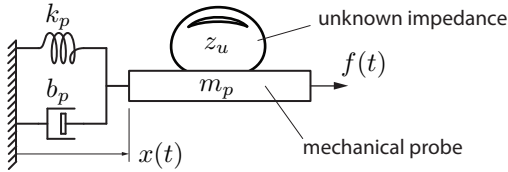


FIG. 1. Principle of operation, illustrated when testing a finger in the tangential direction. The unknown load, z_u , perturbs the response of the probe.

An impedance can be found by comparing the force applied, $F(j\omega)$, to the acceleration $\ddot{X}(j\omega)$, the velocity $\dot{X}(j\omega)$, and the displacement $X(j\omega)$,

$$Z(j\omega) \stackrel{\text{def}}{=} \frac{F}{\ddot{X}}(j\omega) = j\omega \frac{F}{\dot{X}}(j\omega) = -\frac{j}{\omega} \frac{F}{X}(j\omega).$$

If Z_p is known, the unknown load mechanics can be deduced at any frequency from the measured impedance using $b = \Re(Z_u(j\omega))$ and $m\omega - k/\omega = \Im(Z_u(j\omega))$.

This approach is effective only if the impedance of the probe is commensurate with or smaller than that of the load. The smaller is $|z_p|$ before $|z_u|$, the better is the measurement. In this article we describe a closed-loop control approach to reduce the impedance of the probe without suffering from sensor noise amplification.

B. Error Analysis

The unknown impedance, z_u , is calculated from

$$z_u = \frac{f}{\dot{x}} - \frac{f}{\dot{x}_p},$$

where f is the force output from a transducer, \dot{x} the velocity of the probe coupled to the load, and \dot{x}_p the velocity of the unloaded probe. Assuming additive white Gaussian noise in the sensors and a rigid probe, the variance of the measurement can be expressed in terms of individual components by evaluating the propagation of error,

$$\sigma_z^2 = \left(\frac{\sigma_f^2}{f} + \frac{\sigma_{\dot{x}}^2}{\dot{x}} \right) \left(\frac{f}{\dot{x}} \right)^2 + \left(\frac{\sigma_f^2}{f} + \frac{\sigma_{\dot{x}_p}^2}{\dot{x}_p} \right) \left(\frac{f}{\dot{x}_p} \right)^2.$$

If σ_f and $\sigma_{\dot{x}}$ can be considered to be constant, it follows that in order to minimize the variance of σ_z , the unloaded probe displacement should be as high as possible, i.e the probe mobility should be as high as possible,

$$\lim_{x_p \rightarrow \infty} \sigma_z^2 = \left(\frac{\sigma_f^2}{f} + \frac{\sigma_{\dot{x}}^2}{\dot{x}} \right) \left(\frac{f}{\dot{x}} \right)^2.$$

This relationship is at the core of the resonant measurement principle. Low-loss transducers oscillating at resonance have an impedance that is close to zero, displacement is maximized, and the measurement of the load impedance is optimal. At this point, there are two possible paths to follow in order to achieve an active reduction of impedance for any frequency using a single transducer. They are discussed in the next section.

C. Active Feedback Control Approaches

A first approach would be to use feedback to construct a closed-loop system that behaves like a high-Q resonant system whose frequency can be placed arbitrarily. The resonant tuning approach is attractive, but is only applicable over a narrow range. Given a certain physical transducer, forcing the closed-loop system to resonate above the transducer's natural frequency becomes increasingly difficult with rising frequencies, since the input drive signal amplitude must also increase, leading to saturation.

Another inherent limitation comes from the sensitivity behavior of a closed-loop system.²¹ Given G , the system transfer function and C , the feedback, the magnitude of the sensitivity function, $|S| = 1/|(1 + GC)|$, cannot be kept low when $|G|$ becomes small, since there is no freedom in the choice of C . The result is an increasing sensitivity to parameter errors, precluding the achievement of high-Q closed-loop behavior in the high frequencies. Such an approach also limits the measurement options since identification techniques employing random signal excitation are precluded.

Another approach, adopted here, is to employ feedback to reduce the impedance of the closed-loop system over a targeted range of frequencies. If the system impedance can be kept uniformly low in this range, then many measurement options are possible, including the sine sweep excitation technique that is exemplified in this article. Intuitively, the objective is to maximize displacement by

increasing the apparent mobility. The choice of the transducer is therefore critical. Laplace-force transducers or electrostatic force transducers have the desired natural, low-impedance characteristics. At the targeted length-scale (1–10 mm displacements), however, electromagnetic transducer, i.e. the voice-coil is the transducer of choice.

In the control diagram, Fig. 2, $Y_p = 1/Z_p$ represents the mobility of the probe, Z_c the impedance of the active feedback, γ the combined drive factor of the transducer and the gain of the amplifier, u the reference input, and i the current driven in the coil.

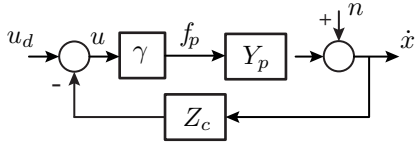


FIG. 2. Closed-loop control. Position, velocity and acceleration are fed back to the transducer to modify the apparent impedance.

The output, \dot{x} , is a combination of sensor noise signal, n , injected in the loop and of the reference signal u_d ,

$$\dot{x} = \frac{\gamma Y_p}{1 + \gamma Y_p Z_c} u_d + \frac{1}{1 + \gamma Y_p Z_c} n.$$

Assuming that the noise from the sensor is zero-mean, Gaussian with variance σ_n^2 , and that the sensor is the dominant source of noise, the measurement variance is

$$\sigma_{\dot{x}}^2 = \left| \frac{1}{1 + \gamma Y_p Z_c} \right|^2 \sigma_n^2,$$

and the mean velocity is

$$\langle \dot{x} \rangle = \frac{\gamma Y_p}{1 + \gamma Y_p Z_c}.$$

The ratio $\sigma_{\dot{x}}/\langle \dot{x} \rangle$ does not change under closed-loop control, hence the measurement is not affected by closing the loop, as long as the feedback does not introduce additional significant errors. The control problem boils down to a pole placement problem to produce a uniform response over a range of frequencies, while achieving a reduction of the apparent impedance of the transducer at a value significantly smaller than that of the load to be measured.

III. IMPLEMENTATION

The concept was applied to the particular case of the measurement of the fingertip impedance. A device, illustrated Fig. 3, was constructed from a voice-coil motor driving a eight-bar flexural guide able to support the pressure of a finger. Since a voice-coil accurately transforms a current into a force, the sensors are expected to

be the dominant source of noise and error. To avoid the need to design a state-observer, sensors directly measuring displacement, velocity and acceleration were included in the design.

A. Electro-Mechanical Arrangement

Referring to Fig. 3 a fingertip was constrained by a holder and was pressed against a surface which was guided by a flexure driven by a voice-coil motor (FRS8, VISATON GmbH, Haan, Germany). A force-sensor (Nano 17, ATI Industrial Automation, Apex, NC, USA) was placed under the ground link of the flexure to monitor the normal force component. It was also used to measure the tangential force component acting on the flexure for calibration the motor drive factor.

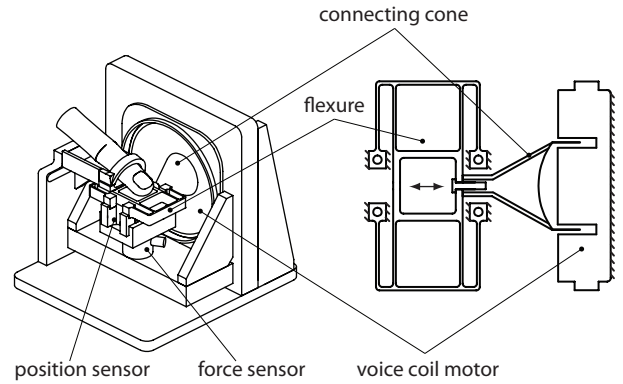


FIG. 3. Mechanical implementation of the impedance-meter.

The flexure was of the eight-bar type which has the benefit of exact compensation of off-axis stresses and which therefore provides accurate linear guidance, even for large deflections.²² It was cut out of acetal plastic.

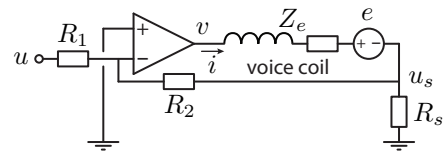


FIG. 4. Current-mode coil drive.

The voice-coil was driven by a voltage-controlled current amplifier in order to compensate for the coil inductance and the back-EMF. The Laplace force generated by the coil was then proportional to the command voltage, u , see Fig. 4. The circuit was built from an operational amplifier (OPA548, Texas Instruments, Dallas, TX, USA) where the feedback was provided by a precision shunt resistance R_s . The transconductance gain was $i/u = -R_2/(R_1 R_s)$. Given a voice-coil with drive factor Bl , the total gain was

$$\gamma = \frac{f}{u} = -Bl \frac{R_2}{R_1 R_s}.$$

B. Impedance feedback control loop

The objective was to reduce the apparent impedance of the system in order to maximize the difference between the unloaded and the loaded configurations. The control was obtained by feeding back position, velocity, and acceleration to the transducer through three gains that respectively modified the apparent stiffness, damping, and mass of the system. The open-loop transfer function in the Laplace domain was

$$\gamma u = (ms^2 + bs + k)x,$$

where m , b and k are the mass, damping coefficient and the stiffness of the actuator, and where s is the Laplace operator. In closed-loop operation, the position, x , the velocity, \dot{x} , and the acceleration, \ddot{x} , were fed back through gains l_k , l_b , and l_m , leading to

$$\gamma u = [ms^2 + bs + k - \gamma(l_ms^2 + l_bs + l_k)]x.$$

The apparent dynamic parameters were

$$\bar{m} = m - \gamma l_m, \quad \bar{b} = b - \gamma l_b, \quad \text{and} \quad \bar{k} = k - \gamma l_k.$$

Thus,

$$Z(s) = \frac{\gamma u}{sx} = Z_p(s) - \gamma Z_c(s), \quad (1)$$

where $Z_c(s) = l_ms^2 + l_bs + l_k$, represents the controller impedance as in Fig. 2. Stability was ensured as long as the apparent dynamic parameters were strictly positive.

The feedback was implemented using analog circuits employing operational amplifiers (LMC660, Linear Technology Corp., Milpitas CA, USA) to compute the gains, sums, and differences that the control required.

C. Sensing

The position sensor was built from a hall-effect sensor (SS49, Honeywell, Morristown, NJ, USA) responding to the magnetic field of a semi-Halbach magnet configuration that created a uniform gradient over a large region. With three 5 mm cuboid neodymium-iron-boron magnets a 4 mm region with a 0.1 T/mm gradient at a distance of 2.5 mm away from the magnets was achieved, see Fig. 5. A finite-element analysis showed good linearity over ± 2 mm range (linear regression with $R^2 > 99.9\%$). This configuration exhibited a five-fold advantage over the convention single-magnet arrangement. The noise floor of the position sensor was 2 μm .

Velocity was measured from the back-EMF generated by the voice-coil. The voltage, v , across the coil terminals and the current, i , flowing through it (through the R_s shunt resistor) were measured. The circuit included the voice-coil electrical impedance, Z_e , in series with a voltage generator, $e = Bl\dot{x}$, and a known voltage generator, v . Kirchhoff's law gives $e = v - [(Z_e + R_s)/R_s]u_s$ from which \dot{x} was easily derived with the analog electronics.

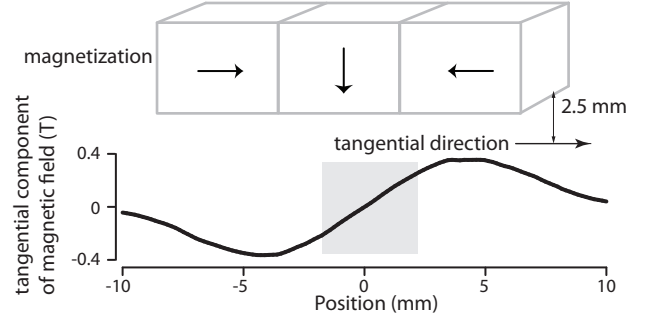


FIG. 5. Magnet arrangement. Arrows point to the magnetization direction. Magnetic field at 2.5 mm away from the surface of the assembly. The gray area shows the region of constant gradient.

A commercially available accelerometer (2250A-10, Endevco, San Juan Capistrano, CA, USA) measured acceleration. Its mass was 0.4 g and its size was $5 \times 10 \times 3$ mm.

D. Control

The resulting system could be represented by a second-order system, but this approximation did not hold in the high frequencies. Since we aimed at wide bandwidth operation, the higher modes reduced or eliminated the stability margin at high gains. Autoregressive identification showed that the actual system could be well approximated by a 6-pole and 2-zero transfer-function from 20 Hz to 10 kHz. The lower two poles accounted for the second order behavior, and the remaining poles and zeros modeled a low-Q anti-resonance around 800 Hz and a sharper resonance at 3 kHz. The frequency response of the system and of the model are shown in Fig. 6.

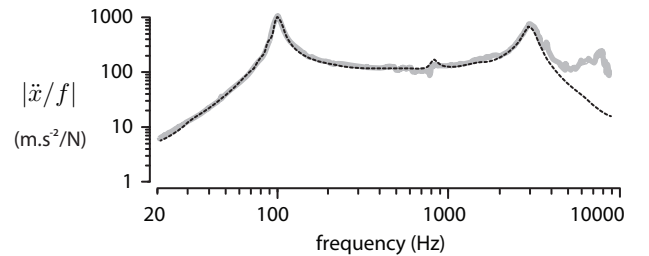


FIG. 6. Mobility response retrieved from the accelerometer (thick gray) and fitted model (dashed).

From this model, the root loci for each feedback gain, acceleration, velocity, and position, were computed, see Fig. 7. Acceleration feedback decreased the apparent mass, but also reduces stability as the other poles moved toward the right-hand-side of the imaginary plane. Velocity feedback reduced the apparent damping. Stability was ensured only when the apparent damping was strictly positive. Position feedback modified the appar-

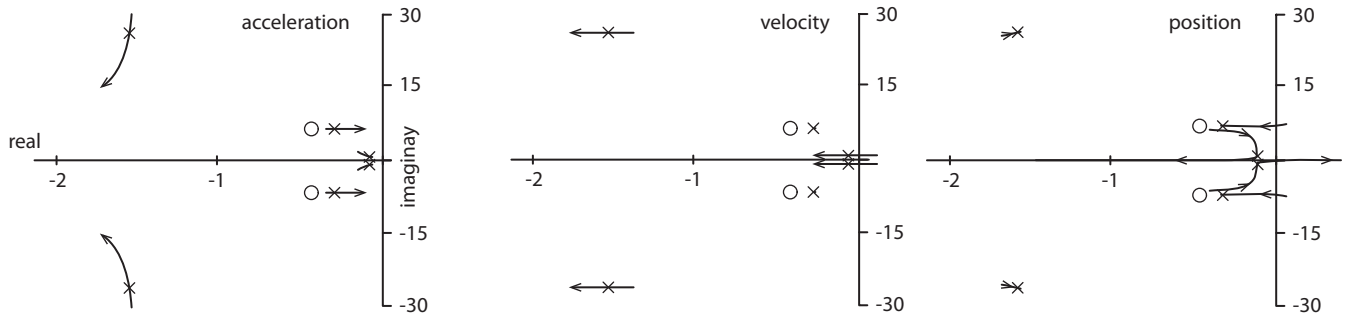


FIG. 7. Root loci. Effects of acceleration, velocity, and position feedback. Arrows show the effect of increasing gains. Crosses and circles are the poles and zeros of the open-loop transfer function, respectively.

ent stiffness. Stability was ensured as long as the apparent stiffness was strictly positive. With the aid of these diagrams, the system was tuned to achieve the response described in the next section.

IV. RESULTS

A. Unloaded closed-loop response

The closed-loop frequency response in the targeted frequency band of the unloaded actuator is shown in Fig. 8, where it can be compared to the original open-loop response. With a 3 dB gain margin on the acceleration feedback, the mobility was increased by a factor 5. The closed-loop acceleration was the same as the acceleration available in open-loop at the natural resonant frequency (i.e. 100 Hz). A limiting factor of the present realization was the 800 Hz resonance. Performance could be increased in future realizations by employing more accurate sensors and by optimizing the structural response of the suspension. Using better materials than acetal plastic it would be possible to push the frequency of the higher modes further away from the natural resonant frequency.

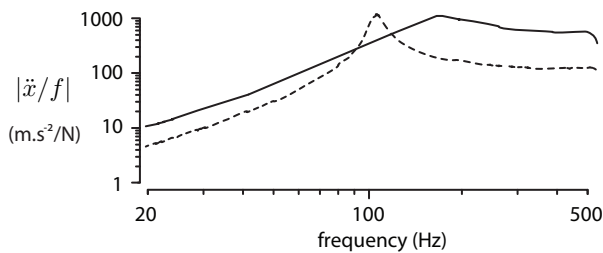


FIG. 8. Instrument response (solid line) and original response (dashed). The impedance is approximately 5 times smaller.

B. Proof masses

Validation was performed using calibrated masses of 0.5 g and 1.25 g. Using sine sweep excitation for the

measurements of the unloaded and loaded response, the impedance in 30-500 Hz band was retrieved, see Fig. 9. The standard variation was evaluated from 50 measurements. These measurements were extracted from the accelerometer signal which is the most accurate of the three sensors used in the system.

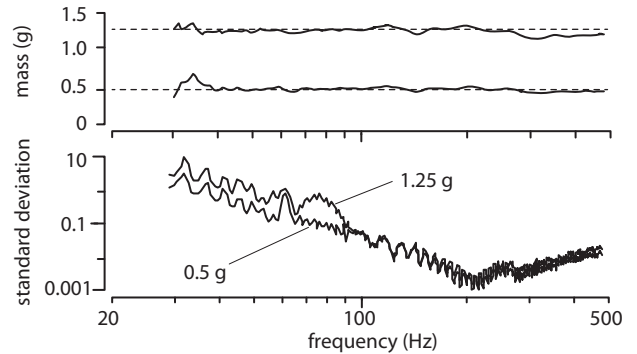


FIG. 9. Proof mass calibration. Standard deviation at all frequencies. Above 80 Hz the measurement of the acceleration error lower than 0.1 g.

Above 100 Hz, measurement errors never exceeded 10%. The standard deviation of the measurement follows the same amplitude pattern as the impedance and the relative acceleration was higher above 80 Hz. The uncertainty in the low frequency is caused by the low relative value of the inertial contribution to the total impedance.

C. Proof cantilever

We fabricated a small elastic cantilever beam out of acetal plastic. Its response was measured independently from an impulsive test using a Doppler-effect vibrometer (OVF-2500 with OVF-534 head, Polytec Inc., Irvine, CA, USA). The tip of the cantilever was bonded to the moving plate of the apparatus using double sided tape and impedance measurements were performed in the 30-500 Hz bandwidth. The results can be seen in Fig. 10. The very low damping of the proof cantilever explain the difference in the results in the high frequencies but the

low frequencies the measurement followed the expected decrease of impedance with a rate of -20 dB/decade. The impedance value dropped around the resonant frequency. In the high frequencies, the impedance measurement showed the expected inertial behavior since the impedance increased at a rate of $+20$ dB/decade.

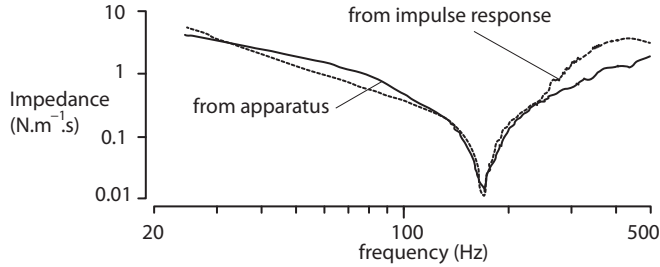


FIG. 10. Measurement of the proof beam. The impedance from the impulse response was obtained from displacement measurement divided by frequency.

D. Fingertip measurement

We can now show an example of a complete mechanical behavior measurement made while touching the probing plate of the instrument with a finger pushing on it with a normal force of 0.6 N, see Fig. 11. In the low frequencies, the probing displacement was of the order of one millimeter.

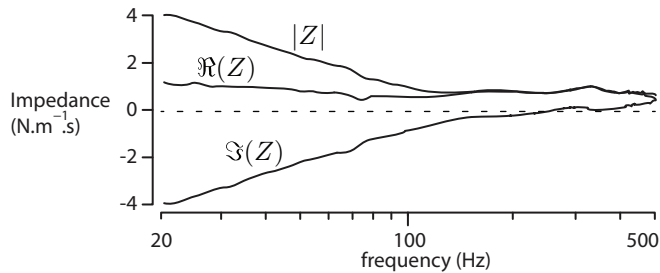


FIG. 11. Complete mechanical characterization of a fingertip.

It can be seen from the absolute value of the measured impedance that the fingertip behaved essentially like a spring, up to a frequency of 100 Hz. Damping, identified from the real part of the impedance, was significant and dominated above 150 Hz. The apparent mass of the fingertip was quite small, viz. 0.2 g, and its contribution to the response results to the change of sign of the imaginary part of the impedance around 250 Hz. However, the real part of the impedance was not significant compared to the damping above 100 Hz. Therefore the finger could be modeled as a spring and a damper, with a transition at about 100 Hz.

These results are consistent with previous observations reporting that the fingertip skin can track unilateral stimuli up to about 100 Hz, albeit with normal excitation,²³

the cited study being the only one which, to our knowledge, has tested the fingertip skin behavior within the full frequency range that we can consider with our apparatus. Other measurements, not reported here, showed that the fingertip impedance varied significantly according to several factors.

V. CONCLUSION

We have described an apparatus able to probe the bulk mechanical impedance of a sample over a wide range, using a single actuator. A feedback loop was used to reduce the apparent impedance of the actuator, producing a state of quasi-resonance at any frequency. From proof masses and a proof cantilever, we could determine that the apparatus could detect a 0.1 g mass within the 20 to 500 Hz range.

The intended application is the measurement of the fingertip mechanical properties. Initial measurements revealed that the fingertip could be modeled by a spring and a damper—a Kelvin element—in the range from DC to 500 Hz, but that the impedance varied according to the testing conditions, a phenomenon which the subject of ongoing investigations.

The closed-loop operation principle for the reduction of apparent impedance, implemented here with a mesoscale electromagnetic device, could be easily extended to larger or smaller devices. In the small scales, electrostatic comb devices would scale favorably for actuation and sensing. Improvements could also result from the use of higher-order feedback and feedforward polynomial-based approaches to compensate for the inevitable mechanical limitations resulting from the higher resonant modes. Field Programmable Gate Arrays (FPGA) digital circuit technology running digital control algorithms at high sampling rates could also replace analog circuits, providing many more control design options and enhanced repeatability. Finally, state observers could be included in the control design to reduce the number of sensors, but their impact on the accuracy of the measurements would have to be investigated.

ACKNOWLEDGMENTS

The authors would like to thank José Lozada for insightful comments. They would also acknowledge the help of Mehdi Boukallel and Mathieu Grossard. This work was supported by the Agence Nationale de la Recherche (ANR) through the REACTIVE project (ANR-07-TECSAN-020). Additional funding was from the European Research Council, Advanced Grant PATCH, agreement No. 247300.

- ¹A. Hajian and R. D. Howe, *Journal of biomechanical engineering* **119**, 109 (1997)
- ²A. Israr, S. Choi, and H. Tan, in *Proceedings of IEEE World Haptics Conference 2007*, pp. 56–60
- ³A. Israr, S. Choi, and H. Tan, in *Proceedings of Intelligent Robots and Systems, 2006*, pp. 472–477
- ⁴K. Kuchenbecker, J. Park, and G. Niemeyer in *Proceeding of the ASME Int. Mechanical Engineering Congress and Exposition*, (2003) Vol. 2 p. 42017
- ⁵J. Dolan, M. Friedman, and M. Nagurka, *IEEE Transactions on Systems, Man and Cybernetics* **23**, 698 (1993)
- ⁶C. Fu and M. Oliver, in *Proceedings of IEEE World Haptics Conference 2005*. pp. 657659
- ⁷M. Mridha and S. Ödman, *The Journal of Investigative Dermatology* **85**, 575 (1985).
- ⁸Q. Wang, L. Kong, S. Sprigle, and V. Hayward, in *Proceedings of the IEEE Engineering in Medicine and Biology Society Conference* (2006) pp. 5997–6000
- ⁹B. Gillespie and M. Cutkosky, in *Proceedings of the ASME Dynamic Systems and Control Division*, (1996) Vol. 58 pp. 397–406
- ¹⁰M. Wiertelwski, J. Lozada, E. Pissaloux, and V. Hayward, in *Proceedings of Eurohaptics 2010*, LNCS, Vol. 6192, edited by A. M. L. Kappers et al. (Springer-Verlag, 2010) pp. 17–24
- ¹¹Q. Wang and V. Hayward, *International Journal of Robotics Research* **29**, 323 (2010)
- ¹²F. Firestone, *The Journal of the Acoustical Society of America* **4**, 249 (1933)
- ¹³G. OHara, *The Journal of the Acoustical Society of America* **41**, 1180 (1967)
- ¹⁴S. Sands, P. Camilleri, R. Breuer, G. Cambrell, R. Alfredson, E. Skuza, P. Berger, and M. Wilkinson, *Journal of Sound and Vibration* **320**, 559 (2009)
- ¹⁵J. Brownjohn, G. Steele, P. Cawley, and R. Adams, *Journal of Sound and Vibration* **73**, 461 (1980)
- ¹⁶O. Doutres, N. Dauchez, J. Genevaux, G. Lemarquand, and S. Mezil, *Review of Scientific Instruments* **81** (2010)
- ¹⁷S. Asif, K. Wahl, and R. Colton, *Review of scientific instruments* **70**, 2408 (1999)
- ¹⁸F. J. Giessibl, *Phys. Rev. B* **56**, 16010 (Dec 1997)
- ¹⁹S. Park, M. Goodman, and B. Pruitt, *Proceedings of the National Academy of Sciences* **104**, 17376 (2007)
- ²⁰J. Acosta, G. Hwang, J. Polesel-Maris, and S. Régnier, *Review of Scientific Instruments* **82**, 035116 (2011)
- ²¹J. C. Doyle, B. A. Francis, and A. Tannenbaum, *Feedback Control Theory* (Macmillan, 1990)
- ²²S. T. Smith, D. G. Chetwynd, and D. K. Bowen, *Journal of Physics E: Scientific Instruments* **20**, 977 (1987)
- ²³J. C. Cohen, J. C. Makous, and S. J. Bolanowski, *Experimental Brain Research* **129**, 211 (1999)